MIT Libraries | DSpace@MIT

MIT Open Access Articles

Elastic averaging for assembly of three-dimensional constructs from elastomeric micromolded layers

The MIT Faculty has made this article openly available. ***Please share*** how this access benefits you. Your story matters.

Citation: Marentis, T.C. et al. "Elastic Averaging for Assembly of Three-Dimensional Constructs From Elastomeric Micromolded Layers." Microelectromechanical Systems, Journal of 18.3 (2009): 531-538. ©2009 IEEE.

As Published: http://dx.doi.org/10.1109/JMEMS.2009.2018372

Publisher: Institute of Electrical and Electronics Engineers

Persistent URL: http://hdl.handle.net/1721.1/60272

Version: Final published version: final published article, as it appeared in a journal, conference proceedings, or other formally published context

Terms of Use: Article is made available in accordance with the publisher's policy and may be subject to US copyright law. Please refer to the publisher's site for terms of use.

Massachusetts Institute of Technology

Elastic Averaging for Assembly of Three-Dimensional Constructs From Elastomeric Micromolded Layers

Theodore C. Marentis, Joseph P. Vacanti, James C. Hsiao, and Jeffrey T. Borenstein

***Abstract*—Precision engineering has been used in the macroworld and in the microscale only with rigid materials. Soft flexible materials commonly used for microfluidics and other bio-MEMS applications have not been aligned with elastic averaging. We report the use of complementary raised and recessed circular features to align polymer layers and demonstrate alignment accuracy and repeatability. The alignment is accomplished in a Petri dish with a thin layer of liquid between the two surfaces of micromolded elastomeric polymer sheets. The layers are aligned with simple hand–eye manipulation. We test circular geometries of varying diameters, obtaining accuracy and repeatability values in the range of 1–3 μm across thin polymer sheets molded from silicon masters. This is a significant improvement over existing manual, moving stage, and self-alignment techniques and a novel proof of concept that paves the way for complex 3-D polymer constructs. [2008-0093]**

***Index Terms*—Alignment, biomedical engineering, elastic averaging, lab-on-a-chip, microassembly, microfluidics, micromachining, poly-(dimethylsiloxane) (PDMS), precision engineering, silicone rubbers, surface fitting, tissue engineering.**

I. Introduction

SOFT LITHOGRAPHY has enabled patterning of features on elastomeric sheets with submicrometer resolution [1]. These polymer constructs can be used in a variety of applications such as microfluidics, lab-on-a-chip, micro total analysis systems (μTAS), chemical electrophoresis systems [2], [3] polymerase chain reaction (PCR) chambers [4], [5], and microfluidic large-scale integration systems including memory chips and comparators [6].

Tissue engineering has adopted soft lithography to pattern biocompatible polymers like poly-(dimethylsiloxane) (PDMS) [7] and biodegradable polymers like poly(lactic-co-glycolic acid) (PLGA) [8] or poly(glycerol-sebacate) (PGS) "biorubber" [9], [10]. PDMS constructs can function as acellular microfluidic devices and perform biological functions such as blood filtration or membrane oxygenation for renal or pulmonary assist [11]. They can function as cell-based, biocompatible extracorporeal assist devices for liver function [12]. Cell seeding enhances their properties such as hemocompatibility [13]. For instance, endothelialization of PDMS microfluidic capillary beds has been shown to reduce their thrombogenicity when in contact with blood [14]. Cells seeded in these artificial microenvironments can also perform complex biological functions that mimic physiologic behavior [15]. Biodegradable polymers create a temporary structure for cell seeding, proliferation, and establishment of biological function, but the polymer degrades and is replaced by living tissue [15].

The majority of soft lithography constructs usually have between one and three polymer layers [16]–[19]. The need for increasing the number of layers accurately positioned over one another is emerging for several microfluidic applications [15]. PCR and μTAS applications require more compact efficient 3-D networks with shorter channel lengths to reduce reagent and sample volumes [6], [20]. In immunology and cell biology, precise control of the planar cellular microenvironment has allowed the study of cell–cell interactions, linking them to protein regulation [21], immunological activation [22], and the effect of mechanotransduction and shear stress on cell behavior [22]. These applications also require recapitulation of cell–cell interactions and cell–matrix interactions that occur in 3-D configurations *in vivo*. Finally, 3-D constructs can facilitate the integration of electrical circuits within microfluidic networks on a single chip [24], [25].

The field of tissue engineering has been successful in creating tissues such as cartilage or skin [26], [27]. Organs with simple 3-D geometry like the bladder have also been demonstrated by sequential addition of cell layers [28]. However, organs with complex 3-D structure, such as the liver and the kidney, have not been realized. The establishment of adequate function requires a cellular volume that is comparable to the original organ. As the organ size increases, blood perfusion with oxygen and nutrients and removal of metabolic waste decline due to increased diffusion length, leading to tissue ischemia and death. A capillary network that can transfer blood directly to the core of an organ is a feasible solution [29] but has so far been limited to pseudo-3-D scaffolds of few layers [Fig. 1(a)].

A pseudo-3-D structure comprises a stack of repeating copies of the same polymer layer. The layers are commonly connected in parallel with a single inlet and outlet in the z-axis. True 3-D

Manuscript received April 6, 2008; revised September 24, 2008 and December 31, 2008. First published May 2, 2009; current version published June 3, 2009. Subject Editor A. Lee.

T. C. Marentis is with the Harvard–MIT Division of Health Sciences and Technology, Cambridge, MA 02139 USA, with the Charles Stark Draper Laboratory, Cambridge, MA 02139-3563 USA, with the Center for Regenerative Medicine, Massachusetts General Hospital, Boston, MA 02114 USA, and also with the Howard Hughes Medical Institute, Chevy Chase, MD 20815 USA (e-mail: marentis@gmail.com).

J. P. Vacanti is with the Center for Regenerative Medicine, Massachusetts General Hospital, Boston, MA 02114 USA, and also with the Department of Pediatric Surgery, Massachusetts General Hospital, Boston, MA 02114 USA.

J. C. Hsiao and J. T. Borenstein are with the Charles Stark Draper Laboratory, Cambridge, MA 02139-3563 USA.

Digital Object Identifier 10.1109/JMEMS.2009.2018372

1057-7157/$25.00 © 2009 IEEE

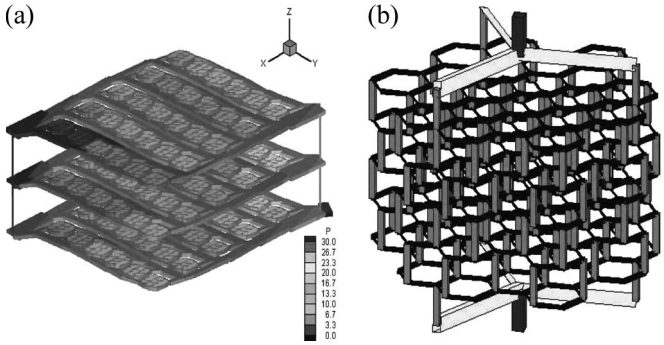

Fig. 1. (a) (Left) Pseudo-3-D scaffold created by stacking copies of the same vascular layer. (b) (Right) True 3-D scaffold. Each layer is distinct and capillaries channel fluid in all three dimensions.

structures comprise layers with distinct features that can have varying connections in the z-axis [Fig. 1(b)]. This allows one to approximate natural or man-made designs more closely.

A common challenge for 3-D constructs composed of individual components is accurate alignment of these components along the x–y plane. Available approaches to address this problem include self-alignment [18], hand alignment under a microscope using recessed alignment marks on both surfaces [19], and moving stages, either manual or mechanical, in combination with a microscope [30]. Accuracy and repeatability are the traditional figures of merit for alignment results. Additional desirable features of the alignment process include the ease of processing, compatibility with a variety of materials, and scalability of both device size and production volume.

With all of these requirements in mind, we explored a technique that is potentially capable of addressing each aspect: precision engineering with flexible polymers. Precision engineering is a subfield of mechanical engineering traditionally used to assemble large structures such as engines [31]. Its use has been extended to MEMS to align solid silicon wafers [32]. Precision engineering can be accomplished either by kinematic coupling or by elastic averaging. Both techniques rely on raised geometries on one surface coming in contact with recessed geometries on the other. In kinematic coupling, point contacts are established between the two surfaces. The minimum number of points is used, which translates to a total of six points, three on each surface, minus the desirable degrees of freedom the system is allowed. Point contacts frequently lead to high point stress concentrations and material fatigue. Due to the limited number of contact points, kinematic coupling is best used with rigid materials [31]–[33].

Elastic averaging requires a greater number of contact points between the two surfaces dispersed over a larger area. This results in an overconstrained system that averages displacement within the material bulk through elastic deformation. The alignment is nondeterministic in that it cannot be mathematically modeled in closed form. Elastic averaging can accommodate very high loads, and performance improves after an initial wear-in period [31], [32]. Elastic averaging is therefore better suited for polymer materials that can deform and average a greater amount of displacement within their bulk. A systematic study of the accuracy and precision of such alignment with flexible polymers has not yet been conducted.

II. Materials and Methods

A. Design

We used the computer-aided design software L-Edit (Tanner, CA) to partition a 4-in wafer into 2 × 2 cm squares. Each square carried two components: an alignment component with either raised or recessed features and a readout component that provides displacement measurements. All design dimensions are summarized in Table I, and our wafer layout is shown in Fig. 3(b).

Our alignment geometries are composed of circles and triangles arranged in a circular pattern. There were a 7 × 7 array of large circles, a 12 × 12 array of intermediate circles, and a 22 × 22 array of small circles. The circles that translated to recessed features had diameters of 2.4 mm, 1.2 mm, and 600 μm. The structures that translated to raised features had diameters of 2.4 mm, 1.2 mm, 1.203 mm, 595 μm, and 600 μm. The combinations of slightly different diameters allowed us to test fits that were loose, exact, and tight. The triangular geometries, as well as the large circular geometries, did not perform to the level of the intermediate or small circular features and will not be discussed further. There were 132 intermediate 1.2-mm circles and 436 small 600-μm circles.

For readouts, we created Vernier scales with staggered triangles [34], [35] (Fig. 2). We designed a low-resolution (1.5-μm) high-dynamic-range (15-μm) scale and a high-resolution (0.5-μm) low-dynamic-range (5-μm) scale. To produce values for the x- and y-axes, we positioned a high- and a low-resolution scale perpendicular to each other. Each scale had two sets of 21 staggered triangles facing tip-to-tip. The triangles of one set had narrow bases of 75 μm, while triangles of the second set had bases 75.5 μm wide in the high-resolution scale and 76.5 μm wide in the low-resolution scale. The midline was referenced with one central triangle taller or shorter than the rest.

When perfectly aligned, only the center triangles line up perfectly [Fig. 2(a)]. If the blocks are misaligned by one base-width difference, the first triangle to the left or right of the central triangle aligns perfectly. For a misalignment of two base widths, the second triangle to the left or right aligns perfectly and so on and so forth [Fig. 2(c)]. Misalignment is measured by identifying the triangle set that points tip-to-tip, counting the number of triangles away from the center one and multiplying it by the base-width difference.

B. Microfabrication

The microfabrication process flow is summarized in Fig. 3(a). The alignment and readout schematics were printed on high-resolution transparency masks using a 5080 dpi system (Heidelberg Herkules Imagesetter, Heidelberg, Germany). We spun a positive-tone photoresist (Shipley 1822, Rohm and Haas, Philadelphia, PA) (Headway PWM32, Headway Research Inc., Garland, TX) on 4-in 550-μm-thick silicon wafers (Si-Tech, Topsfield, MA), soft baked and exposed in hard contact mode using a Suss MA6 mask aligner (Suss MicroTec Inc., Waterbury, VT). The wafers were developed in Microposit MF319 bath (Microchem Corporation, Newton, MA), hard

TABLE I
DESIGN GEOMETRIES AND DIMENSIONS

Circular Alignment Geometries			Vernier Read-out Triangles			
Array	Reccesed	Raised	Location	Number	Base Width	Height
	Diameter					
7 x 7	2.4 mm	2.4 mm	Set 1 Center	1	75 µm	80 µm
12 x 12	1.2 mm	1.2 mm	Set 1 Adjacent	20	75 µm	100 µm
		1.203 mm	Set 2 Center	1	75 µm	140 µm
22 x 22	600 µm	595 µm	Set 2 Adjacent	20	Coarse: 76.5 µm	120 µm
		600 µm			Fine: 75.5 µm	

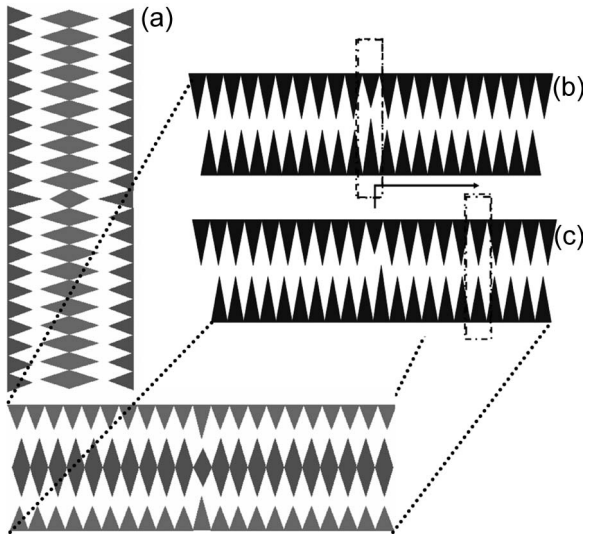

Fig. 2. (a) (Left and bottom) Two readout ends superimposed. (b) (Top right) Perfect alignment. The upper triangles belong to one layer, while the lower ones belong to the other. Only the central pair of triangles is perfectly aligned due to the small difference in base width. (c) (Center right) Misalignment by 9 μm. The sixth pair of triangles lines up perfectly. Multiply the width difference of 1.5 μm by 6 to get 9-μm misalignment.

baked and plasma ashed. We etched the exposed silicon with the Bosch deep silicon etch process for a depth of 20 μm (STS Standard Rate ICP-ASE, Surface Technology Systems, Newport, U.K.). The wafers were stripped of their photoresist in SVC-14 (Rohm and Haas, Philadelphia, PA) and cleaned in piranha etch (3 : 1 H_2SO_4 : H_2O_2).

For the alignment features, we used AZ P4620 (AZ Electronic Materials USA, Somerville, NJ). The soft- and hard-bake times were the same. We exposed for 20 s and developed in AZ400K (AZ Electronic Materials USA, Somerville, NJ). In two of the four wafers, we aimed for a 100-μm etch depth, and in the other two, a 150-μm depth.

C. Soft Lithography

Polydimethylsiloxane (PDMS) prepolymer and a curing agent (SYLGARD 184 Silicone Elastomer Kit, Dow Corning, Midland, MI) were mixed in a 10 : 1 ratio by weight. The prepolymer mixture was degassed. We positioned the silicon molds in a Petri dish and poured an approximately 7-mm-thick layer of liquid PDMS over each mold. We allowed the PDMS to cure in a 65 °C oven (Blue M Electric, Watertown, WI). We peeled the PDMS off the mold and cut along the lines separating the 2 × 2 cm squares [Fig. 3(c)].

D. Alignment

We rotated one of the two squares 180° about the y-axis [Fig. 3(c)]. We rinsed the surfaces of the two polymers with 95% ethanol to create a thin liquid layer between them and brought them in contact in a Petri dish [Fig. 3(d)]. This was accomplished without a microscope for the 2.4- and 1.2-mm-diameter circles. For the 600-μm-diameter circles, we performed coarse alignment of the layers with hand–eye manipulation first and then used low-power magnification (5x) for fine alignment. The two blocks were pressed against each other to bring the raised and recessed figures together and allow for elastic averaging to take place.

E. Data Acquisition

We examined the three readout squares in each block under a light microscope (Olympus SZx12) at 50x magnification. A digital image was captured with a camera (3CCD T45C 0.45x) and stored in tiff format (Q-Capture Pro) (Fig. 4). We identified the two triangles pointing tip-to-tip that were perfectly aligned, counted how many triangles they were away from the midline, and recorded it in MS Excel. The polymer blocks were taken apart and put together again, and the same process repeated five times.

F. Data and Statistical Analysis

Accuracy was calculated as the root mean square of all alignment values [31]. Displacement data from fine and coarse Vernier scales of all three readout squares were averaged separately for each axis for all repetitions to produce an x- and y-axis block alignment accuracy. There are two acceptable ways to measure repeatability: the standard deviation of the distance from the desired position [31] and the range of the data divided by two, after removing two extreme outliers [36]. We used both of these methods but removed only one outlier due to a smaller number of data points.

We produced P values by using one-sided paired t-tests to compare alignment performance of the x-axis to the y-axis, the 100-μm-tall features to the 150-μm ones, and the 1.2-mm-diameter circles to the 600-μm ones. One-sided t-tests assuming equal variances compared the central readout squares to the peripheral ones. The underlying assumptions for choosing a one-sided t-test are that the y-axis performs better than the x-axis, as will be discussed, and that the greater the number of alignment features and the taller their height, the better the alignment. We also assume that alignment improves in a central

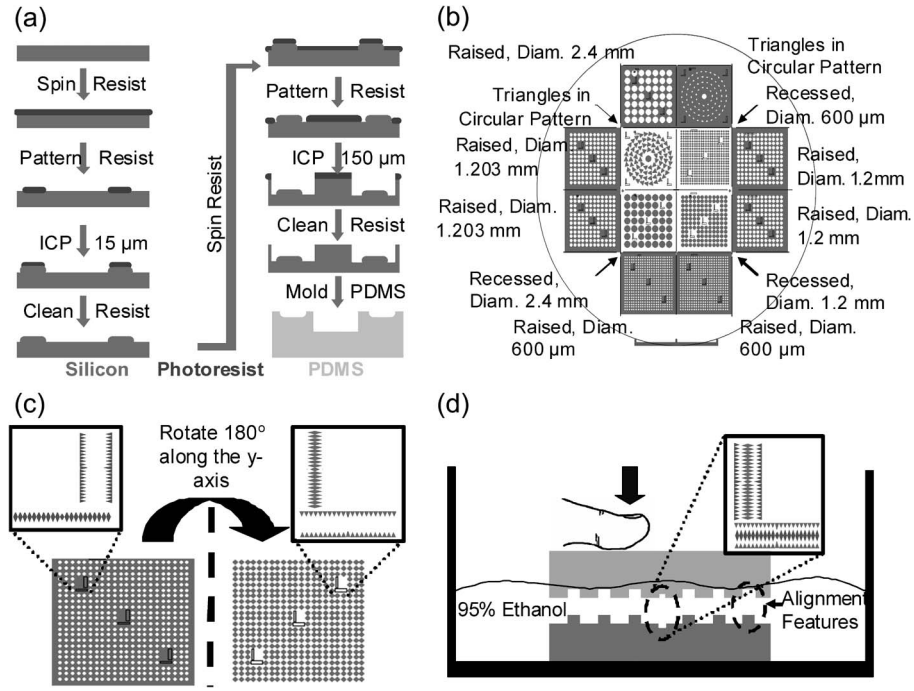

Fig. 3. (a) (Top left) Microfabrication process. The Vernier scales are created with a 15-μm ICP etch and the alignment features with a 150-μm etch. (b) (Top right) Wafer layout. Raised and recessed features are manufactured on the same wafer, molded to PDMS, and individual squares are diced. (c) (Bottom left) Complementary alignment features and Vernier scales on PDMS prior to alignment. One square is rotated 180° about the y-axis. (d) (Bottom right) Alignment with hand–eye manipulation over a thin liquid medium. The blocks are gently pushed onto each other. The Vernier scales come together.

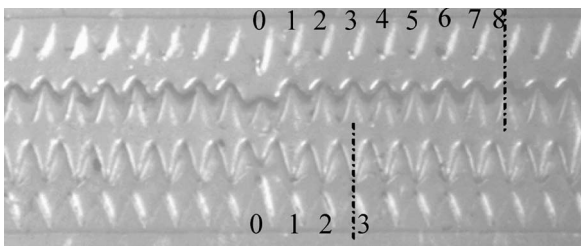

Fig. 4. Raw data from two Vernier scales. The top scale is the fine scale and aligns perfectly eight triangles off the center for a misalignment of 4 μm (8×0.5 μm). The lower scale is the coarse scale. It aligns three triangles off the center for a misalignment of 4.5 μm (3×1.5 μm).

location surrounded by many alignment features rather than a peripheral location.

III. Results and Discussion

All data collected are summarized in Table II. It is important to note that the relatively small sample sizes used to collect data in Table II create the potential for large effects from outlier data points. In order to address this, we have dropped one data point from the calculation of repeatability that is shown in the table. The alignment accuracy in the x-axis was worst than that of the y-axis ($P = 0.046$). However, repeatability was better for the x-axis ($P = 0.014$), whereas both axes had similar standard deviations ($P = 0.29$). We attributed the discrepancy in accuracy to an inherent error of the system. Our Suss MicroTec MA6/ 8NFH mask aligner aligns the second mask to the silicon wafer with an error of 0.5 μm for front-to-front processes [37]. Both raised and recessed features come from the same mold,

TABLE II
Alignment Absolute Accuracy, Repeatability, and Standard Deviation in Micrometers of Different Diameter Alignment Features

Diameter		Height	Axis	Accuracy	Repeatability	Std. Dev
Recessed	Raised	(μm)				
1.2mm	1.2mm	100	X	2.2	3.7	4.0
			Y	1.8	4.8	4.6
		150	X	5.8	2.0	4.9
			Y	0.6	2.1	2.0
1.2mm	1.203mm	100	X	9.3	1.5	4.1
			Y	5.6	2.5	3.6
		150	X	1.6	1.6	4.1
			Y	1.6	5.1	3.6
600μm	595μm	100	X	4.5	0.9	2.4
			Y	1.5	2.5	2.9
		150	X	12.2	1.3	3.0
			Y	4.8	1.1	4.9
600μm	600μm	100	X	0.1	0.3	2.4
			Y	3.4	0.6	1.6
		150	X	9.1	0.6	3.9
			Y	1.2	2.3	3.4

and bringing them in contact requires a 180° rotation about the y-axis [Fig. 3(c)]. This doubles the error in the x-axis while canceling it in the y-axis. In the future, we can use molds from the same wafer positioned over each other without a rotation in a way that cancels the error on both axes. Our analysis of accuracy will therefore focus exclusively on the y-axis.

We present the alignment geometries as triplets of numbers followed by x or y for the axis, such as 600-600-100-x, that refer to the recessed feature diameter, the raised feature diameter, and their height/depth in micrometers. The two best configurations were the 1.2-mm-diameter 150-μm-tall pairs with accuracy of 0.6 μm, repeatability of 2.1 μm, and standard

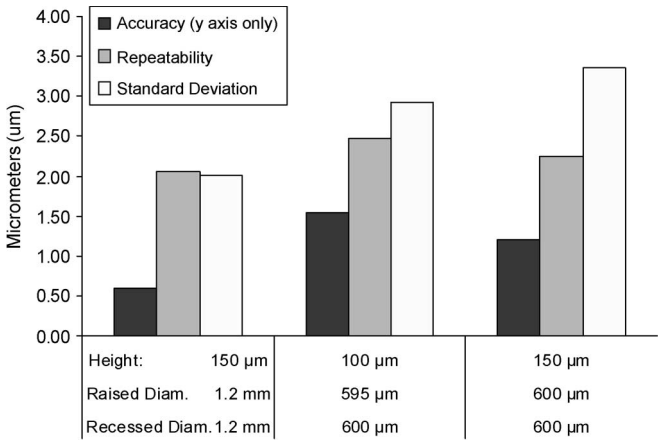

Fig. 5. Accuracy, repeatability, and standard deviation of alignment of three top performing alignment feature pairs.

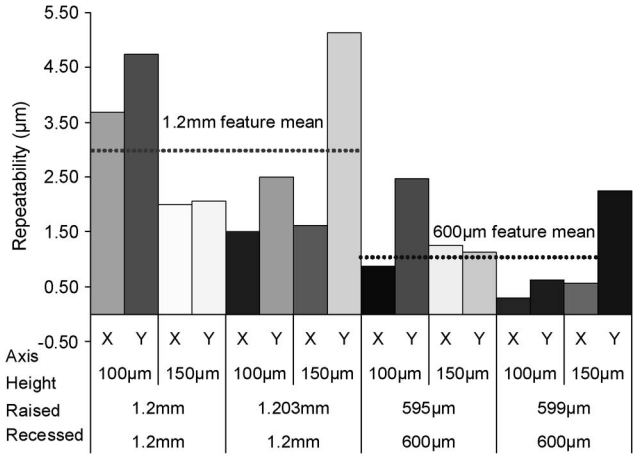

Fig. 6. Repeatability of features with 1.2-mm and 600-μm diameters demonstrating the improved performance of the 600-μm features ($P = 0.0004$).

deviation of 2.0 μm, and the 600-μm-diameter 100-μm-tall pairs with accuracy of 0.1 μm, repeatability of 0.3 μm, and standard deviation of 1.6 μm (Fig. 5).

The theory behind elastic averaging states that alignment accuracy and repeatability improve with the square root of the number of contact points [31]. However, the theory has been difficult to support with experimental evidence [32]. We did not observe a difference between alignments with 132 large 1.2-mm features and 436 small 600-μm ones in accuracy ($P = 0.121$) and standard deviation ($P = 0.109$). However, the 600-μm features produced a significant improvement in repeatability over their 1.2-mm counterparts ($P = 0.0004$) with an average repeatability of 1.18 μm as compared to 2.91 μm (Fig. 6). This is an improvement over the expected repeatability (Fig. 7) probably explained by the increased percentage of surface area covered by the smaller alignment features.

Exact fit pairs appeared to have better accuracy, repeatability, and lower standard deviation than tight fit, but the difference was not statistically significant (accuracy: $P = 0.342$, repeatability: $P = 0.376$, and standard deviation: $P = 0.488$). The exact fit pairs appeared also to have better accuracy than the loose fit but, again, not statistically significant (accuracy:

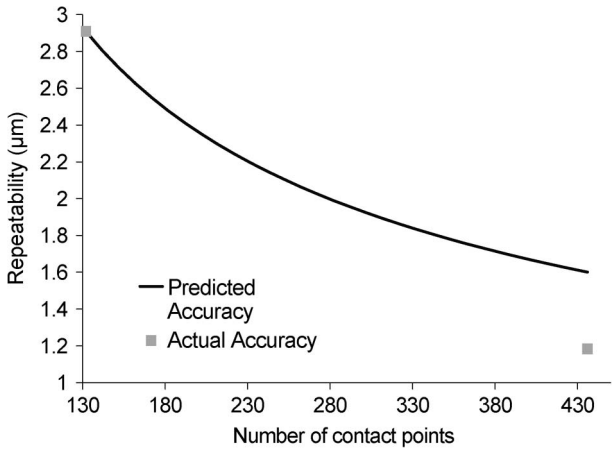

Fig. 7. Predicted and actual repeatability depending on the number of alignment features.

$P = 0.440$, repeatability: $P = 0.238$, and standard deviation: $P = 0.217$). This was attributed to the limited number of data points as well as the very small difference in diameters. The 150-μm-tall features did not provide a clear advantage over the 100-μm ones (accuracy: $P = 0.23$, repeatability $P = 0.48$, and standard deviation: $P = 0.40$).

The ubiquitous use of Vernier scales made them a straightforward choice for our experiments. Macroworld Vernier calipers achieve resolutions of 20 μm, and in the microworld, resolutions are as low as 0.1 μm [34], [35], [38]. As they are so commonly used in the field and our resolutions were 0.5 and 1.5 μm, we did not experimentally reevaluate their accuracy.

One potential limitation of the precision of this experiment relates to the use of a Mylar mask, which has a resolution of 5080dpi or approximately 1 dot per 5 μm, to measure alignment in the single micrometer range. There are several considerations that mitigate the influence of the low-resolution mask on the findings of this study, including the inherent properties of repeatability, the size of the features relative to mask resolution, averaging of the linear resolution over the second dimension in the plane, and repeating design in combination with bulk deformation averaging.

For repeatability, mask resolution is not a salient consideration because the measurement focuses on how close the observations are to one another, and therefore, a deviation between the actual mask feature size and the target feature size does not enter into the analysis. The alignment geometries are either 1200 or 600 μm in diameter, three orders of magnitude greater than 5-μm resolution. During photoresist exposure and development, the original pixels on the mask with a linear resolution of 5080 dpi on the x-axis are smoothened over the y-axis into continuous lines with higher resolution than that of the original mask. Even if one feature is 1 μm shorter or longer than desired, the repeating nature of the design in combination with material bulk averaging compensates in the next features. All these factors enable improved accuracy of feature definition and the overall pattern with a much tighter control than the mask resolution suggests, and alignment accuracy and repeatability in single and submicrometer range.

Regarding the potential issue of run-out error, the mask generation technique does not result in a large run-out error but simply a random error in individual feature size. For the PDMS elastomer, the layers are thick enough that stretching is minimal, and therefore, the run-out error on the elastomer features is also very limited. For thin layers (less than 50 μm in thickness), this would become a more significant consideration in determining accuracy of the technique.

Work by other laboratories has focused on hand, moving stage, and self-alignment techniques. In [38], a moving stage and a microscope system are used to align PDMS layers. No actual values are quoted, but the SEMs presented suggest an accuracy of 20–25 μm. In [16], polyurethane (PU) layers are manually stacked with tweezers and a stereoscope. This allows for "...high ($\sim$10–25 μm) accuracy...," with no repeatability data. In [39], a sophisticated polymer aligner based on a stereo microscope and a set of x–y–z micrometer stages produces an accuracy of ± 10 μm, without documented repeatability. In [18], a liquid layer of methanol trapped between two polymer layers is used for alignment. The surface tension of the methanol and coarse hand alignment under low-power magnification produce accuracy of 15 μm.

In addition to alignment accuracy, there are numerous other advantages of precision-engineered alignment. Prior techniques are based on the visualization of alignment geometries, which is impossible with opaque polymers like the PGS biorubber. This is also not feasible when a membrane separates two polymer layers [11], [40], but it is possible with precision engineering that is not based on visualization. Moreover, visualization becomes increasingly more difficult as the number of polymer layers increases, errors are additive, and scale-up and mass production become increasingly challenging [41]. No such limitation exists for elastic averaging. An alternative technique is 3-D printing [42]. However, this approach has limited utility because the smallest droplet that can be printed is approximately 45 μm [42], much greater than photolithography resolution and the alignment achieved here.

Elastic averaging enables the transition to true 3-D structures [Fig. 1(b)] of multiple layers. We have used this alignment technique to align vascular layers with a minimum dimension capillary width of 24 μm into stacked 3-D structures with great success [Fig. 8(a)]. Alignment is accurate to the extent that two layers do not appear distinct unless when visualized at an angle [Fig. 8(b)].

Such scaffolds lend themselves to three key applications that we hope to pursue in the immediate future: liver, muscle, and nerve regeneration. Specifically, the liver has a complex 3-D configuration of lobules [43] and receives 28% of the cardiac output, more than any other organ [43]. Therefore, three-dimensionality and vascularization are essential [15]. Beating cardiac muscle patches have been limited to 100–200-μm thickness, insufficient for clinical applications [45], [46]. The limiting factor is the 100-μm oxygen diffusion length. Channels in PGS spaced on the x–y plane to account for the oxygen diffusion limit have increased the viability of cardiac patches [46]. Precision engineering is a reasonable next step approach to increasing patch thickness of 3-D PGS scaffolds. Finally, neuronal regeneration approaches based on conduits created from 2-D polymer layers rolled onto themselves [47] could greatly benefit from the accuracy, repeatability, and scalability of this technology.

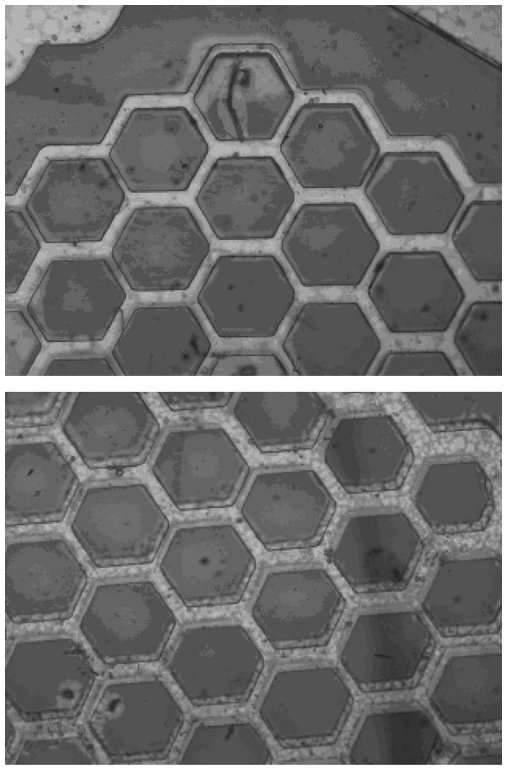

Fig. 8. (a) (Top) Microscopy of two vascular layers aligned over each other. Frontal view. The smallest channels are 24 μm wide. (b) (Bottom) Angled view demonstrating the actual presence of two vascular layers.

IV. Conclusion

We have demonstrated the efficacy of precision engineering elastic averaging in an elastic polymer sheets and achieved submicrometer accuracy and repeatability, superior to self-alignment, hand alignment, and mechanical stage alignment approaches. This alignment process overcomes fundamental barriers associated with visualization-based and self-alignment techniques. Elastic averaging technology is applicable to the manufacture of tissue engineering scaffolds, microfluidics, lab-on-a-chip, and a variety of other applications.

Acknowledgment

The authors would like to thank C. Cardoso, M. Bancu, M. Healey, D. Pulver, E. Weinberg, R. Caruso, B. Orrick, and C. Sundback and also the Charles Stark Draper Laboratory, the Massachusetts General Hospital and the Howard Hughes Medical Institute for supporting this research.

References

[1] D. C. Duffy, J. C. McDonald, O. J. A. Schueller, and G. M. Whitesides, "Rapid prototyping of microfluidic systems in poly(dimethylsiloxane)," *Anal. Chem.*, vol. 70, no. 23, pp. 4974–4984, Oct. 1998.

[2] A. Manz and H. Becker, Eds., *Microsystem Technology in Chemistry and Life Sciences*. Berlin, Germany, Springer-Verlag, 1998.

[3] S. Effenhauser, G. J. M. Bruin, A. Paulus, and M. Ehrat, "Integrated capillary electrophoresis on flexible silicone microdevices: Analysis of DNA restriction fragments and detection of single DNA molecules on microchips," *Anal. Chem.*, vol. 69, no. 17, pp. 3451–3457, Sep. 1997.

[4] J. Khandurina, T. E. McKnight, S. C. Jacobson, L. C. Waters, R. S. Foote, and J. M. Ramsey, "Integrated system for rapid PCR-based DNA analysis in micro fluidic devices," *Anal. Chem.*, vol. 72, no. 13, pp. 2995–3000, Jul. 2000.

[5] E. T. Lagally, I. Medintz, and R. A. Mathies, "Single-molecule DNA amplification and analysis in an integrated microfluidic device," *Anal. Chem.*, vol. 73, no. 3, pp. 565–570, Feb. 2001.

[6] T. Thorsen, S. J. Maerkl, and S. R. Quake, "Microfluidic large-scale integration," *Science*, vol. 298, no. 5593, pp. 580–584, Oct. 2002.

[7] J. T. Borenstein, H. Terai, M. R. Kaazempur-Mofrad, and J. P. Vacanti, "Microfabrication technology: A new tool for vascularized tissue engineering," *Ann. Biomed. Eng.*, vol. 29, p. 154, Oct. 2001. suppl. 1.

[8] M. T. Duailibi, S. E. Duailibi, C. S. Young, J. D. Bartlett, J. P. Vacanti, and P. C. Yelick, "Bioengineered teeth from cultured rat tooth bud cells," *J. Dent. Res.*, vol. 83, no. 7, pp. 523–528, Jul. 2004.

[9] Y. D. Wang, G. A. Ameer, B. J. Sheppard, and R. Langer, "A tough biodegradable elastomer," *Nat. Biotechnol.*, vol. 20, no. 6, pp. 602–606, Jun. 2002.

[10] C. Fidkowski, M. R. Kaazempur-Mofrad, J. Borenstein, J. P. Vacanti, R. Langer, and Y. Wang, "Endothelialized microvasculature based on a biodegradable elastomer," *Tissue Eng.*, vol. 11, no. 1/2, pp. 302–309, Feb. 2005.

[11] M. R. Kaazempur-Mofrad, J. P. Vacanti, and J. T. Borenstein, "A MEMS-based renal replacement system," in *Proc. Solid-State Sensor, Actuator Microsyst. Conf.*, Jun. 2004, pp. 67–70.

[12] A. Cararro, W. M. Hsu, K. M. Kulig, W. S. Cheung, M. L. Miller, E. J. Weinberg, E. F. Swart, M. Kaazempur-Mofrad, J. T. Borenstein, J. P. Vacanti, and C. Neville, "In vitro analysis of a hepatic device with intrinsic microvascular-based channels," *Biomed. Microdevices*, vol. 10, no. 6, pp. 795–805, Dec. 2008.

[13] S. Kaihara, J. Borenstein, R. Koka, S. Lalan, E. R. Ochoa, M. Ravens, H. Pien, B. Cunningham, and J. P. Vacanti, "Silicon micromachining to tissue engineer branched vascular channels for liver fabrication," *Tissue Eng.*, vol. 6, no. 2, pp. 105–117, Apr. 2000.

[14] M. Shin, K. Matsuda, O. Ishii, H. Terai, M. Kaazempur-Mofrad, J. Borenstein, M. Detmar, and J. P. Vacanti, "Endothelialized networks with a vascular geometry in microfabricated poly(dimethyl siloxane)," *Biomed. Microdevices*, vol. 6, no. 4, pp. 269–278, Dec. 2004.

[15] A. Khademhosseini, R. Langer, J. T. Borenstein, and J. P. Vacanti, "Microscale technologies for tissue engineering and biology," *Proc. Nat. Acad. Sci. USA*, vol. 103, no. 8, pp. 2480–2487, Feb. 2006.

[16] A. Folch, S. Mezzour, M. Düring, O. Hurtado, M. Toner, and R. Müller, "Stacks of microfabricated structures as scaffolds for cell culture and tissue engineering," *Biomed. Microdevices*, vol. 2, no. 3, pp. 207–214, Jun. 2000.

[17] P. W. Green, R. R. A. Syms, and E. M. Yeatman, "Demonstration of three-dimensional microstructure self-assembly," *J. Microelectromech. Syst.*, vol. 4, no. 4, pp. 170–176, Dec. 1995.

[18] B.-H. Jo, L. M. Van Lerberghe, K. M. Motsegood, and D. J. Beebe, "Three-dimensional micro-channel fabrication in polydimethylsiloxane (PDMS) elastomer," *J. Microelectromech. Syst.*, vol. 9, no. 1, pp. 76–81, Mar. 2000.

[19] K. R. King, C. C. J. Wang, M. R. Kaazempur-Mofrad, J. P. Vacanti, and J. T. Borenstein, "Biodegradable microfluidics," *Adv. Mater.*, vol. 16, no. 22, pp. 2007–2012, Nov. 2004.

[20] J. S. Marcus, W. F. Andersos, and S. R. Quake, "Parallel picoliter RT-PCR assay using microfluidics," *Anal. Chem.*, vol. 78, no. 3, pp. 956–958, Feb. 2006.

[21] A. Rosenthal, A. Macdonald, and J. Voldman, "Cell patterning chip for controlling the stem cell microenvironment," *Biomaterials*, vol. 28, no. 21, pp. 3208–3216, Jul. 2007.

[22] T. K. Hsiai, S. K. Cho, P. K. Wong, M. Ing, A. Salazar, A. Sevanian, M. Navab, L. L. Demer, and C. M. Ho, "Monocyte recruitment to endothelial cells in response to oscillatory shear stress," *FASEB J.*, vol. 17, no. 12, pp. 1648–1657, Sep. 2003.

[23] D. T. Chiu, N. L. Jeon, S. Huang, R. S. Kane, C. J. Wargo, I. S. Choi, D. E. Ingber, and G. M. Whitesides, "Patterned deposition of cells and proteins onto surfaces by using three-dimensional microfluidic systems," *Proc. Nat. Acad. Sci. USA*, vol. 97, no. 6, pp. 2408–2413, Mar. 2000.

[24] G. Y. Zhang, D. Mann, L. Zhang, A. Javey, Y. Li, E. Yenilmez, Q. Wang, J. P. McVittie, Y. Nishi, J. Gibbons, and H. Dai, "Ultra-high-yield growth of vertical single-walled carbon nanotubes: Hidden roles of hydrogen and oxygen," *Proc. Nat. Acad. Sci. USA*, vol. 102, no. 45, pp. 16141–16145, Nov. 2005.

[25] Y. G. Sun, S. Kim, I. Adesida, and J. A. Rogers, "Bendable GaAs metal-semiconductor field-effect transistors formed with printed GaAs wire arrays on plastic substrates," *Appl. Phys. Lett.*, vol. 87, no. 8, pp. 083 501-1–083 501-3, Aug. 2005.

[26] L. E. Niklason and R. Langer, "Prospects for organ and tissue replacement," *J. Amer. Med. Assoc.*, vol. 285, no. 5, pp. 573–576, Feb. 2001.

[27] V. Yannas, E. Lee, D. P. Orgill, E. M. Skrabut, and G. F. Murphy, "Synthesis and characterization of a model extracellular matrix that induces partial regeneration of adult mammalian skin," *Proc. Nat. Acad. Sci. USA*, vol. 86, no. 3, pp. 993–997, Feb. 1989.

[28] A. Atala, S. B. Bauer, S. Soker, J. J. Yoo, and A. B. Retik, "Tissue-engineered autologous bladders for patients needing cystoplasty," *Lancet*, vol. 367, pp. 1241–1246, Apr. 2006.

[29] National Institute of Biomedical Imaging and Bioengineering, *Tissue Engineering/Regenerative Medicine Meeting Summary, NIH NIBIB 2005*, Jun. 2005. [Online]. Available: http://www.nibib.nih.gov/nibib/File/Research/2005NIBIBWorkshopSummary.pdf

[30] S. S. Kim, H. Utsunomiya, J. A. Koski, B. M. Wu, M. J. Cima, J. Sohn, K. Mukai, L. G. Griffith, and J. P. Vacanti, "Survival and function of hepatocytes on a novel three-dimensional synthetic biodegradable polymer scaffold with an intrinsic network of channels," *Ann. Surg.*, vol. 228, no. 1, pp. 8–13, Jul. 1998.

[31] A. H. Slocum, *Precision Machine Design*. Dearborn, MI: Prentice–Hall College Div., 1992.

[32] A. H. Slocum and A. C. Weber, "Precision passive mechanical alignment of wafers," *J. Microelectromech. Syst.*, vol. 12, no. 6, pp. 826–834, Dec. 2003.

[33] A. H. Slocum and A. Donmez, "Kinematic couplings for precision fixturing—Part 2: Experimental determination of repeatability and stiffness," *Precis. Eng.*, vol. 10, no. 3, pp. 115–122, Jul. 1988.

[34] F. Ericson, S. Greek, J. Soderkvist, and J.-A. Schweitz, "High-sensitivity surface micromachined structures for internal stress and stress gradient evaluation," *J. Micromech. Microeng.*, vol. 7, no. 1, pp. 30–36, Mar. 1997.

[35] Y. B. Gianchandani and K. Najafi, "Bent-beam strain sensors," *J. Microelectromech. Syst.*, vol. 5, no. 1, pp. 52–58, Mar. 1996.

[36] S. D. Senturia, *Microsystem Design*. Boston, MA: Kluwer, 2000, p. 161.

[37] Suss MicroTec, *MA6/ 8NFH Near Field Holography*, Jun. 2006. [Online]. Available: http://www.suss.com/main.php?rad_id=351&rad_f=162

[38] F. Ayazi, "The HARPSS process for fabrication of precision MEMS inertial sensors," *Mechatronics*, vol. 12, no. 9/10, pp. 1185–1199, Nov./Dec. 2002.

[39] J. R. Anderson, D. T. Chiu, R. J. Jackman, O. Cherniavskaya, J. C. McDonald, H. Wu, S. H. Whitesides, and G. M. Whitesides, "Fabrication of topologically complex three-dimensional microfluidic systems in PDMS by rapid prototyping," *Anal. Chem.*, vol. 72, no. 14, pp. 3158–3164, Jul. 2000.

[40] N. L. Jeon, D. T. Chiu, C. J. Wargo, H. Wu, I. S. Choi, J. R. Anderson, and G. M. Whitesides, "Design and fabrication of integrated passive valves and pumps for flexible polymer 3-dimensional microfluidic systems," *Biomed. Microdevices*, vol. 4, no. 2, pp. 117–121, May 2002.

[41] J. T. Borenstein, E. J. Weinberg, B. K. Orrick, C. Sundback, M. R. Kaazempur-Mofrad, and J. P. Vacanti, "Microfabrication of three-dimensional engineered scaffolds," *Tissue Eng.*, vol. 13, no. 8, pp. 1837–1844, Aug. 2007.

[42] H. Seitz, W. Rieder, S. Irsen, B. Leukers, and C. Tille, "Three-dimensional printing of porous ceramic scaffolds for bone tissue engineering," *J. Biomed. Mater. Res. B*, vol. 74B, no. 2, pp. 782–788, Aug. 2005.

[43] W. Ekataksin and K. Wake, "Liver units in three dimensions: Organization of argyrophilic connective tissue skeleton in porcine liver with particular reference to the 'compound hepatic lobule'," *Amer. J. Anat.*, vol. 191, no. 2, pp. 113–153, Jun. 1991.

[44] W. F. Ganong, "Review of medical physiology," in *Lange Medical Books*, 20th ed. Chicago, IL: McGraw-Hill, 2001.

[45] S. Gerecht-Nir, M. Radisic, H. Park, C. Cannizzaro, J. Boublik, R. Langer, and G. Vunjak-Novakovic, "Biophysical regulation during cardiac development and application to tissue engineering," *Int. J. Dev. Biol.*, vol. 50, no. 2/3, pp. 233–243, Mar. 2006.

[46] M. Radisic, W. Deen, R. Langer, and G. Vunjak-Novakovic, "Mathematical model of oxygen distribution in engineered cardiac tissue with parallel channel array perfused with culture medium containing oxygen carriers," *Amer. J. Physiol., Heart. Circ. Physiol.*, vol. 288, no. 3, pp. 1278–1289, Nov. 2004.

[47] T. A. Hadlock, C. A. Sundback, D. A. Hunter, J. P. Vacanti, and M. L. Cheney, "A new artificial nerve graft containing rolled Schwann cell monolayers," *Microsurg.*, vol. 21, no. 3, pp. 96–101, May 2001.

Theodore C. Marentis received the B.S. degree in biomechanical engineering with distinction and the M.S. degree in electrical engineering from Stanford University, Stanford, CA, in 2003, and the M.D. degree (*cum laude*) from the Harvard Medical School, Harvard–MIT Division of Health Sciences and Technology, Cambridge, in 2008. He is currently pursuing medical internship at the New York Downtown Hospital, New York, and a radiology residency program at the University of Michigan, Ann Arbor.

He was a Research Assistant with Stanford University and the Charles Stark Draper Laboratory, Cambridge, MA. He has authored or coauthored five publications and has one patent application. His research interests include MEMS, tissue engineering, biomedical devices, interventional radiology, and imaging.

Dr. Marentis is a Howard Hughes Medical Institute and a P.D. Soros Fellow. He is a member of Tau Beta Pi and Phi Beta Kappa.

Joseph P. Vacanti received the medical degree with high distinction from the University of Nebraska College of Medicine, Omaha, in 1974, and the M.S. degree from Harvard University, Cambridge, MA.

He is currently the John Homans Professor in Surgery at Harvard Medical School, Boston, MA. In addition, he serves as Surgeon in Chief and Chief of Pediatric Surgery at the Massachusetts General Hospital for Children, Boston. He is a Cofounder and Editor of the journal *Tissue Engineering*. He has been working in the field of tissue engineering since its beginnings in the early 1980s—a mission that stems from his long-held interest in solving the problem of organ shortages. His approach to developing tissue involves a scaffold made of an artificial biodegradable polymer, seeding it with living cells, and bathing it in growth factors. The cells can come from living tissue or stem cells. The cells multiply, filling up the scaffold, and growing into a 3-D tissue. Once implanted in the body, the cells recreate their proper tissue functions, blood vessels grow into the new tissue, the scaffold melts away, and lab-grown tissue becomes indistinguishable from its surroundings.

Dr. Vacanti is a member of the American College of Surgeons, American Pediatric Surgical Association, American Society of Transplant Surgeons, and Tissue Engineering Society in addition to many others. He was recently the recipient of the Thomas Sheen Award, presented by the New Jersey Chapter of the American College of Surgeons, and the John Scott Award, which was presented by the city of Philadelphia. The John Scott Award is given to "the most deserving" men and women whose inventions have contributed in some outstanding way to the "comfort, welfare, and happiness" of mankind.

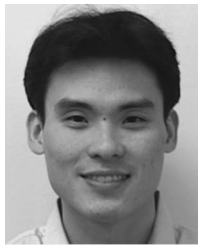

James C. Hsiao received the B.S. degree in mechanical engineering from the Massachusetts Institute of Technology, Cambridge.

From 1999 to 2004, he was with Corning IntelliSense, developing optical gyroscopes, pressure sensors, and MEMS micromirrors. He is currently a member of the MEMS Fabrication Group at the Charles Stark Draper Laboratory, Cambridge, MA, researching inertial sensors, nanoproducts, RF resonators, and tissue engineering scaffolds. He is the holder of one patent and is the coauthor of four publications. His research interests include MEMS processes and their applications in biomedical engineering.

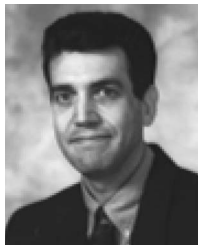

Jeffrey T. Borenstein was born in Baton Rouge, LA. He received the B.S., M.S., and Ph.D. degrees in physics from the University at Albany, Albany, NY, while simultaneously working at North American Philips Corporation on the development of novel electronic materials for the semiconductor industry.

He is currently a Distinguished Member of Technical Staff at the Charles Stark Draper Laboratory, Cambridge, MA. Prior to joining the Draper Laboratory, he was a Solar Cell Fabrication Manager with a division of Mobil Oil Corporation. He has 12 issued patents and another 12 patent applications in the fields of MEMS fabrication technology, inertial MEMS sensors, tissue engineering, and drug delivery. He has supervised six M.S. and six Ph.D. students at the Massachusetts Institute of Technology, Cambridge, and currently directs several programs, developing new technologies for the pharmaceutical and medical device industries. His current research interests focus on the development of tools for drug discovery, organ assist devices, and implantable drug delivery systems.